Association of Dysplastic Coronoid Process with Long-Face Morphology

T. Chen, Z. Liu, C. Xue, W. Tian, D. Bai, and Y. Chen

Appendix

Antibody information:

Primary antibodies used in the study were:

1. Anti-Runx2 1:300 (IHC-P), Santa Cruz, sc-390351;
2. Anti-Pax9 1:500 (IHC-P), Abcam, ab-28538;
3. Anti-HA 1:300 (IHC-P), Abcam, ab-9110;
4. Anti-MF20 1:50 (IHC-P), Novus Biologicals, MAB4470;
5. Anti-mGFP 1:1000 (IHC-P), Abcam, ab-290.

Secondary antibodies, all from Thermo Fisher Scientific and used at 1:500 dilution, were: donkey-anti rabbit (A21207-Alexa Fluor 594, A21206-Alexa Fluor 488, and A32795-Alexa Fluor Plus 647), donkey-anti rat (A21209-Alexa Fluor 647), and donkey-anti mouse (A21202-Alexa Fluor 488 and A32787-Alexa Fluor Plus 647).

Materials and Methods:

Geometric morphometric (GM) analysis

To quantify and analyze the differences in geometric morphometry, GM analysis was conducted using R package Geomorph_3.1.2 (Adams, D. C., M. L. Collyer, and A. Kaliontzopoulou. 2019. Geomorph: Software for geometric morphometric analyses. R package version 3.1.0. https://cran.r-project.org/package=geomorph.). The form of each human mandible was represented by 15 landmarks, of which two representing the furthest point on the condylar process and coronoid

process from the base, respectively, were treated as fixed anatomical landmarks and the other 13 as semilandmarks along the mandibular contour. The placement of semi-landmarks is performed by using Geomagic Studio (3D Systems, USA). The resulting 10 configurations of 15 landmarks were superimposed by a Generalized Procrustes Analysis that standardizes the landmark configurations for the overall position, scale, and orientation, yielding a set of shape coordinates for each sample. The differences between the group mean forms were analyzed by a principal component analysis (PCA) of the average rescaled shape coordinates, among which the individual configurations were projected onto the two principal components (PCs) of the mean forms.

The form of each murine mandible was represented by 20 landmarks, of which two representing the furthest point on the condylar process from the base and the furthest distobuccal point on the alveolar bone of the first mandibular molar, were treated as fixed anatomical landmarks and the remaining 18 as semilandmarks along the mandibular contour. The subsequent procedures were proceeded the same as the human mandibles as described above.

In situ hybridization

In situ hybridization was performed with the RNAscope Intro Pack 2.5 HD Reagent Kit Brown-Mm (Advanced Cell Diagnostics, 322371) according to the manufacturer's instructions. Probe information is as below: *Fgf8* probe (RNAscope Probe-Mm-*Fgf8*, 313411). All experiments were repeated at least three times.

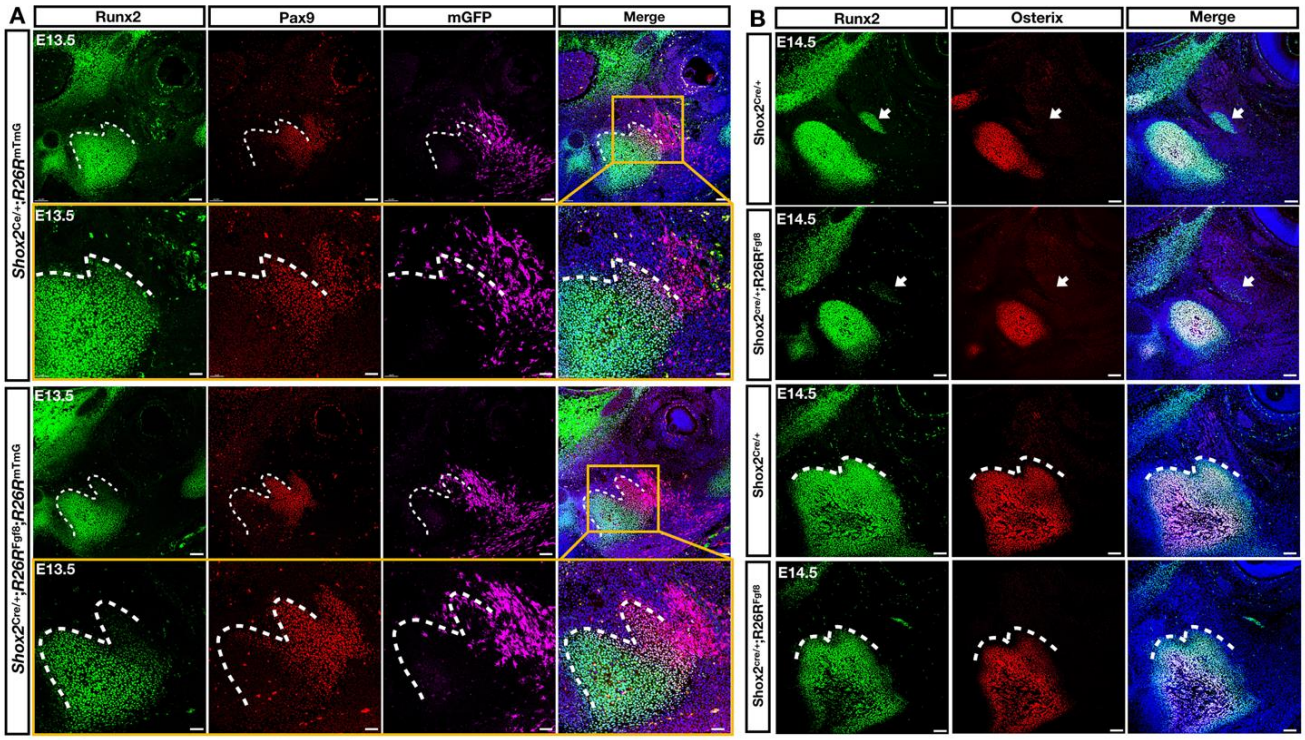

Appendix Figure 1. Enhanced FGF8 signaling disrupts the expression of osteogenic genes. (A) Triple-immunofluorescent staining on sections of the coronoid process of control and *Shox2*$^{Cre/+}$;*R26R*^{Fgf8};*R26R*^{mTmG} mice at E13.5 show the expression levels of Runx2 (green), Pax9 (red), and mGFP (violet). Note that the Runx2 expression is remarkably downregulated in the coronoid process of *Shox2*$^{Cre/+}$;*R26R*^{Fgf8};*R26R*^{mTmG} mice compared to controls. (B) Double-immunofluorescent staining on sections of the coronoid process of control and *Shox2*$^{Cre/+}$;*R26R*^{Fgf8} mice at E14.5 show the expression levels of Runx2 (green) and Osterix (red). Along with the decreased expression level of Runx2, Osterix expression is significantly downregulated in the coronoid process of *Shox2*$^{Cre/+}$;*R26R*^{Fgf8} mice compared to controls. Dotted line delineates the mesenchymal condensation of the mandible. White arrows point to the mesenchymal condensation of the coronoid process. Scale bars = 100-µm (A-upper panels); = 50-µm (A-lower panels, B).

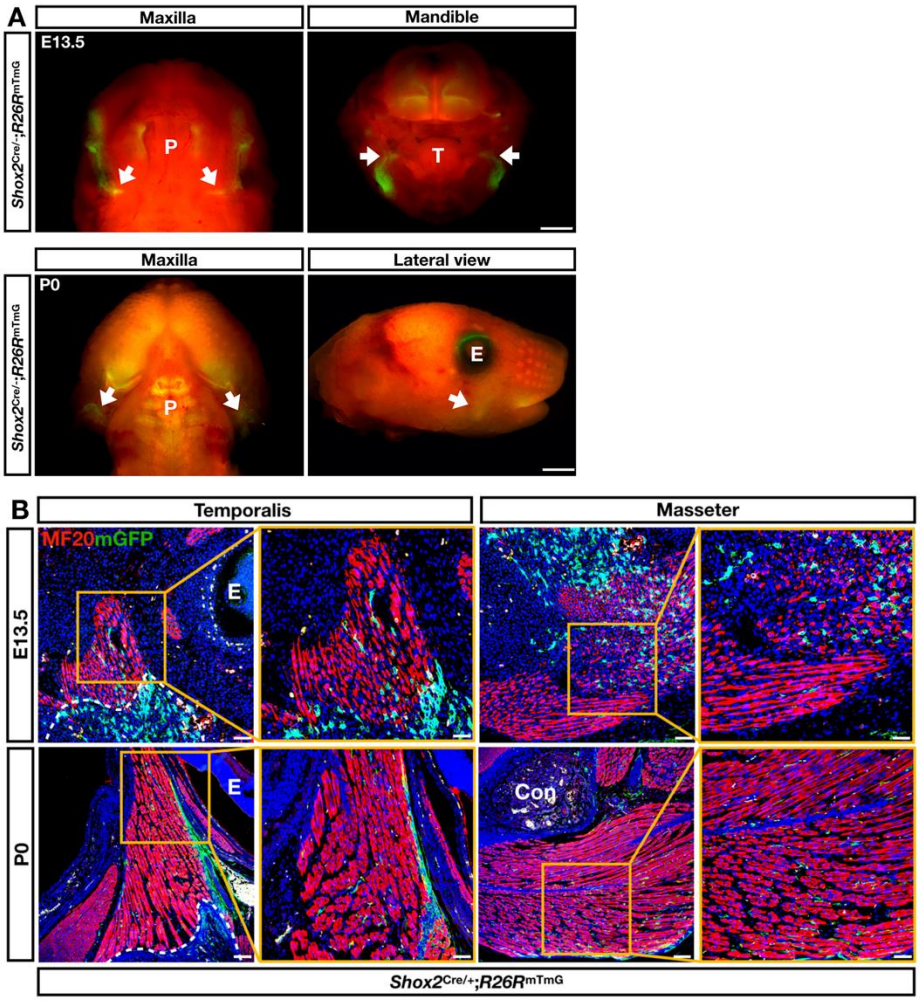

Appendix Figure 2. Lineage tracing of *Shox2*$^{+}$ cells in the craniofacial region and muscle tissue. (A) Whole-mount fluorescent images of E13.5 and P0 *Shox2*$^{Cre/+}$;*R26R*^{mTmG} maxilla (oral view) and mandible (oral view at E13.5 and lateral view at P0) reveal the localization of *Shox2*$^{+}$ cells in the palatine process of the maxilla and the mandibular junction region where the mandibular coronoid process derives from. (B) Double immunostaining on the sections of the *Shox2*$^{Cre/+}$;*R26R*^{mTmG} muscle tissues shows expression patterns of MF20 (red) and mGFP (green) at E13.5 and P0. Note a relatively restricted localization of *Shox2*$^{+}$ cells in the coronoid process without overlapping with muscle tissues including the temporalis and masseter. The white arrows point to the mandibular junction region. Dotted line delineates the mesenchymal condensation of the mandible. Scale bars = 1-mm (A-lower panels); =100-μm (A-upper panels, B-left panels); = 50-μm (B-right panels). P, palate; T, tongue; E, eye; Con, condylar process.

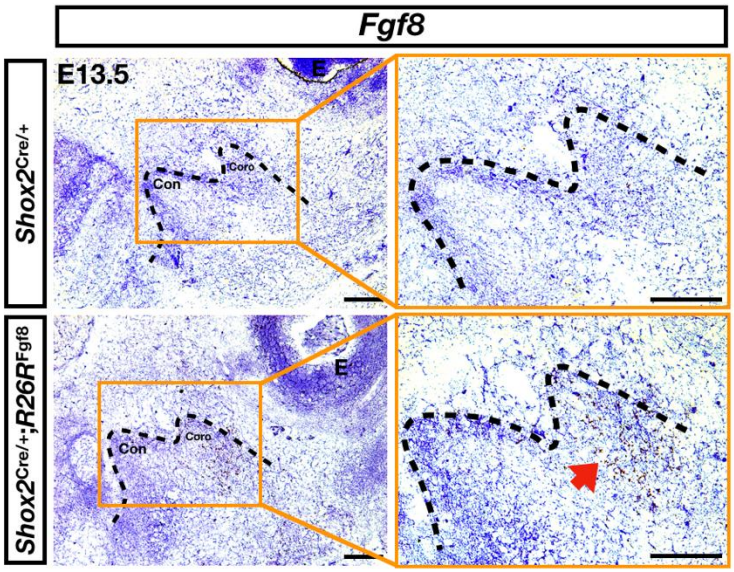

Appendix Figure 3. Ectopic *Fgf8* expression is induced in the mandibular coronoid process of *Shox2*$^{Cre/+}$;*R26R*^{Fgf8} mice. In situ hybridization of *Fgf8* on the sections of control and *Shox2*$^{Cre/+}$;*R26R*^{Fgf8} mandibles at E13.5. Note that the expression of *Fgf8* is ectopically induced in the coronoid process of *Shox2*$^{Cre/+}$;*R26R*^{Fgf8} mice compared to controls. Dotted line delineates the mesenchymal condensation of the mandible. The red arrow points to the brown signals of *Fgf8* in the coronoid process. Scale bars = 100-μm. Con, condylar process; Coro, coronoid process; E, eye.

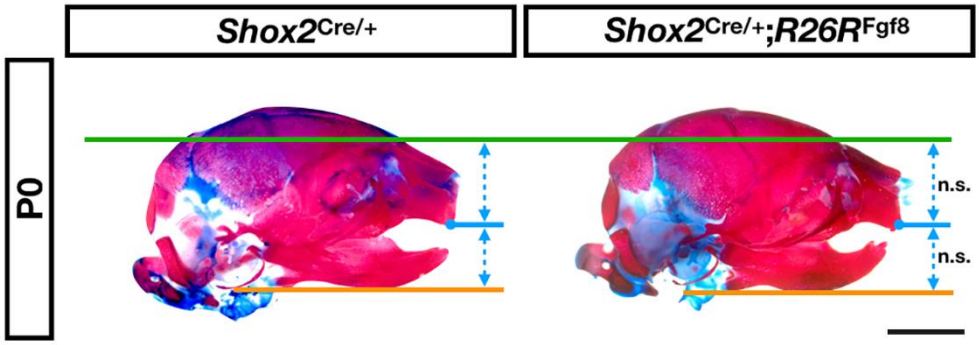

Appendix Figure 4. The normal facial vertical pattern in control and *Shox2*$^{Cre/+}$;*R26R*^{Fgf8} mice at birth. Whole-mount skeletal preparations of control and *Shox2*$^{Cre/+}$;*R26R*^{Fgf8} heads at P0 show the comparable craniofacial vertical pattern in both groups. The measurements of the vertical pattern

analysis show no significant difference between controls and mutants (n = 3 for each phenotype). The green line indicates the reference plane (OIS-E). The blue line indicates the maxillary plane (Mu-Pr). The yellow line indicates the mandibular plane (Gn-Me). n.s.: no statistical significance. Scale bars = 2-mm.

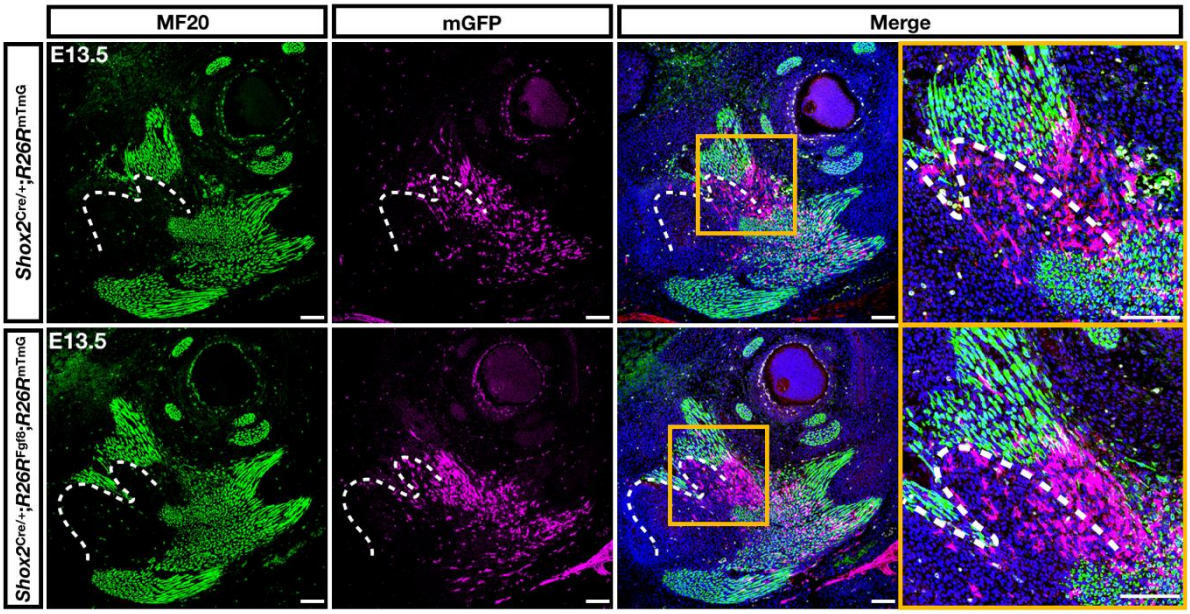

Appendix Figure 5. *Shox2*$^{Cre/+}$;*R26R*^{Fgf8} animals do not exhibit impaired initial development and differentiation of temporal muscle. Immunostaining on sections of the temporal muscle and coronoid process of control and *Shox2*$^{Cre/+}$;*R26R*^{Fgf8};*R26R*^{mTmG} mice at E13.5 shows the expression of muscle-specific marker MF20 (green) and mGFP (violet). The expression level of MF20 is identical in both groups, indicating unaffected muscle development and differentiation. Dotted line delineates the mesenchymal condensation of the mandible. Scale bars = 100-μm.

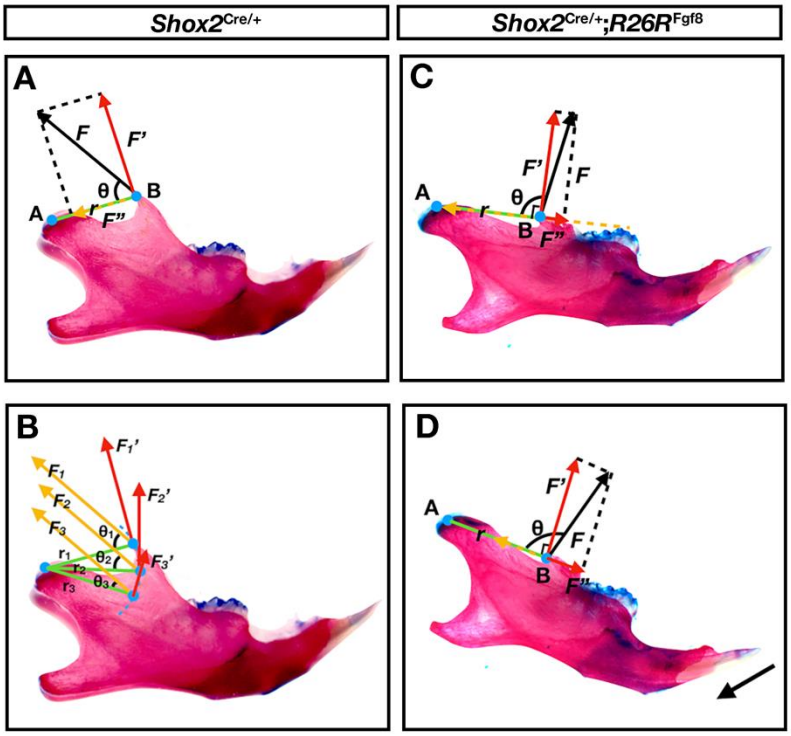

Appendix Figure 6. A model to simulate changes in muscle efficiency with alterations in the morphology of the coronoid process. (A) Biomechanical analysis of the efficiency of the temporal muscle contraction during mandibular movement of control. Note the reference line (marked as ***r***) is created by connecting the condylar process point A and the coronoid process point B. Contraction of the temporal muscle generates a force ***F*** that can be divided into two components based on the reference line: a vertical component (***F'***) and a horizontal component (***F"***). θ is the angle between the direction of ***F*** and ***r***, which also represents the angle of the temporalis relative to the cranial base. (B) Simulation modeling of the relationship between the coronoid process morphology and efficiency of vertical temporal muscle contraction. In this model, we assume that there exist three forces $\boldsymbol{F_1}$, $\boldsymbol{F_2}$ and $\boldsymbol{F_3}$ that share the same magnitude, direction, and force arm. As the point of application moves downwards, the angle θ becomes smaller ($\theta_1 > \theta_2 > \theta_3$) and ***F'*** varies accordingly ($\boldsymbol{F_1'} > \boldsymbol{F_2'} > \boldsymbol{F_3'}$). Thus, the impaired morphology of the mandibular coronoid process may lead to compromised vertical muscular contraction efficiency of the temporalis. (C) Biomechanical analysis of the efficiency of the temporal muscle contraction during mandibular movement of

Shox2$^{Cre/+}$;*R26R*^{Fgf8} mice. Note ***F*** is significantly decreased due to the reduced muscle cross-sectional area in *Shox2*$^{Cre/+}$;*R26R*^{Fgf8} mice. In order to provide enough force to sustain the normal position of the mandible, the orientation of the temporalis fiber has to adopt a vertical direction, which would increase ***F'*** to its maximum to enhance the vertical muscular contraction efficiency. (D) Simulation modeling of the efficiency of the temporal muscle contraction during mandibular clockwise rotation of the *Shox2*$^{Cre/+}$;*R26R*^{Fgf8} mice. Note when ***F'*** fails to provide sufficient support for the vertical load by the mandibular weight, the mandible would generate a clockwise rotation, accelerating LF morphology formation. The black arrow indicates the direction of mandible rotation.

Appendix Table. 1 Landmarks and measurements on the lateral cephalometric for mouse.

Landmark name	Symbol	Comments
E point	E	Intersection between frontal bone and most supers-anterior point of the posterior limit to the ethmoid bone
Gnathion	Gn	Lowest point of the Ramus, or of the angular process
menton	Me	Lowest point on mandibular corpus
Mu point	Mu	The lowest point of the mesial alveolar process of upper M1
Pr point	Pr	The most anterior and lower point if the vestibular alveolar process of the incised bone
O.I.S.	OIS	Occipito-interparietal suture
U1 point	U1	The mesial buccal cusp occlusal point of maxillary first molar
L1 point	L1	The mesial buccal cusp occlusal point of mandibular first molar
U3 point	U3	The mesial buccal cusp occlusal point of maxillary third molar
L3 point	L3	The mesial buccal cusp occlusal point of mandibular third molar
mandibular-plane angle	OISE-GnMe°	Indicator of vertical facial types
Line OIS-E	OIS-E	Reference line
Line U'1-L'1	U'1-L'1	Linear measurement from U1 to L1 relative to the reference line OIS-E
Line U'3-L'3	U'3-L'3	Linear measurement from U3 to L3 relative to the reference line OIS-E
Line Mu-Pr	Mu-Pr	Linear measurement from Mu to Pr indicates maxilla position relative to reference line
Upper Anterior Face Height	E-Mu	Linear measurement from E point to Mu point
Lower Anterior Face Height	Mu-Me	Linear measurement from Mu point to Menton

Appendix Table. 2 Landmarks and measurements on the lateral cephalometric for human patients.

Landmark name	Symbol	Comments
A ponit (subspinale)	A	Most concave point of anterior maxilla
B ponit (supramentale)	B	Most concave point on mandibular symphysis
nasion	N	Most anterior point on frontonasal suture
menton	Me	Lowest point on mandibular symphysis
orbital	Or	Most inferior point on margin of orbit
sella	S	Midpoint of sella turcica
gnathion	Gn	Most outward and everted point on the profile curvature of the symphysis of the mandible
A point-nasion-B point angle	ANB	The relative position of the maxilla to mandible
sella-nasion-A point angle	SNA	The horizontal position of the maxilla relative to the cranial base
sella-nasion-B point angle	SNB	The horizontal position of the mandible relative to the cranial base
Frankfort mandibular-plane Angle	FH-MP (FMA)	Indicator of vertical facial types
Y Axis-SN (Gnathion - Sella - Nasion)	Y-axis	An estimate of mandibular growth direction
Upper Anterior Face Height	N-ANS	Linear measurement from Nasion to Anterior Nasal Spine
Lower Anterior Face Height	ANS-Me	Linear measurement from Anterior Nasal Spine to Menton
Total Face Height	N-Me	Linear measurement from Nasion to Menton
	N-ANS/N-Me	Ratio of linear measurement N-ANS to N-Me
	ANS-Me/N-Me	Ratio of linear measurement ANS-Me to N-Me

Appendix Table. 3 Landmarks and measurements of the mandibular coronoid process for human patients.

Landmark name	Symbol	Comments
C point	C	The deepest point of mandibular norch
Cor point	Cor	The furthest point on the coronoid process from the coronoid base
D point	D	The posterior point of the coronoid process
E point	E	The midpoint of C and D
F point	F	The intersection of the Frankfort plane and Cor-E line
G point	G	The midpoint of C' and D'
H point	H	The midpoint of coronoid length
Line A	Line A	A line perpendicular to the Frankfort horizontal plane through point D
Line B	Line B	A line perpendicular to the Frankfort horizontal plane through point P.
Line C'D'	C'D'	The length of the line parallel to CD through the midpoint of the coronoid length
Coronoid curvature	E-G-Cor angle	he angle formed at point G between the lines drawn from G to Cor and E.
Coronoid angle		the intersection of the Frankfort horizontal plane and the Cor–E line.
Coronoid notch depth		the perpendicular distance between lines A and B
Coronoid length		the distance from point Cor to t E between C and D on line CD
Coronoid width		the length of the line C'D' parallel to CD through H